8-2014

Development of sulfur cathode material for Li-S batteries.

Ruchira Ravinath Dharmasena
University of Louisville

DEVELOPMENT OF SULFUR CATHODE MATERIAL FOR Li-S BATTERIES

By

Ruchira Ravinath Dharmasena
Bsc. University of Peradeniya, Sri Lanka

A Thesis
Submitted to the Faculty of the
College of Arts and Sciences of the University of Louisville
In Partial Fulfillment of the Requirements
For the Degree of

Master of Science

Department of Physics
University of Louisville
Louisville, Kentucky

August 2014

DEVELOPMENT OF SULFUR CATHODE MATERIAL FOR Li-S BATTERIES

By

Ruchira Ravinath Dharmasena
Bsc. University of Peradeniya, Sri Lanka

A Thesis Approved on

June 30, 2014

By the Following Thesis Committee

_____
Dr. G. Sumanasekara (Thesis Director)

_____
Dr. C.S.Jayanthi

_____
Dr. H.R.Gutierrez

_____
Dr. S.McNamara

DEDICATION

This thesis is dedicated to my dearest wife

Dilshani Ranasinghe

Whose support was always invaluable

ACKNOWLEDGEMENT

Finally I would like to thank the UofL Conn Center Renewable energy staff for offering me support when ever wanted and my lab colleagues for making the lab an enjoyable place to work.

ABSTRACT

DEVELOPMENT OF SULFUR CATHODE MATERIAL FOR Li-S BATTERIES

Ruchira Ravinath Dharmasena

June 30th 2014

Efforts were taken to fabricate a cathode material having Sulfur as the active material. First step is composed of identifying potential ways of fabricating a stable and efficient platform for cathode using Reduced Graphene Oxide and activated Multiwall Carbon Nanotubes. The characteristics of those materials are not subjected to detailed discussions, but their synthesis processes are described and results are shown. Some of the previously attempted works on fabricating a Sulfur cathode material are also reattempted in the lab and their results are also shown. Here, a chemical approach is taken rather than physical approach to develop a Sulfur cathode material. A new approach is attempted to fabricate a Sulfur cathode material using Organo Sulfur compounds. Fabricated Sulfur cathodes were tested with respect to Lithium anode and Discharging/Charging curves, Cyclic Voltammetry and voltage variation upon charging/discharging are analyzed.

TABLE OF CONTENTS

LIST OF TABLES

LIST OF FIGURES

CHAPTER 1

INTRODUCTION

Motivation

It is an inconvenient truth that the fossil fuel deposits are depleting at an alarming rate. Therefore scientists are searching for new energy sources such as renewable energy. Solar cell energy and wind energy are major alternative energy sources in this regard. However storing energy is equally important as producing energy. Electricity has become the energy source in modern world. Almost all the energy forms are eventually converted into electricity. In this respect storing electrical energy has been a subject of research interests for many decades. Currently, Lithium ion batteries remain as the most popular electric energy storing device. However Lithium ion batteries have limitations such as their low capacity and low cyclability. According to the current technology of Li-ion battery systems, they possess initial capacities of 200 mAh/g. Most commonly Li-ion batteries are used in mobile electronic devices, electric vehicles and space instruments. Electric vehicle industry has become one of the leading figures to overcome the limitations of current battery technology. Full electric vehicles are now being manufactured around the world but their performances are limited by the low capacity of the batteries. Intensive research is underway around the world to improve the capacity and the cyclability with minimum capacity loss. Li-S battery technology is an alternative and better candidate to increase the range and power of electric vehicles. According to

the current experiments on Li-S batteries, they have initial charging capacity of 5-7 times the Li ion batteries [1]. But they are still in experimental stage and this thesis presents novel methods of fabricating Sulfur cathodes which helps to Li-S batteries to achieve high charge capacities with in the theoretical limits.

Historical Background of Li Cells

Since Allessandro Volta (1971) invented the first operational battery using Copper and Zinc, the hunger for improved energy storage capabilities has never ended and going to be continued with new innovations. Li element has given necessary push on designing battery with high capacity and compatibility. Experimentation of Li batteries started in 1912 by G.N Lewis and in 1970 the first Li based battery was sold. In 1980 an American scientist, John B. Goodenough found $LiCoO_2$ cathode and a French scientist Richard Yasami discovered the Graphite anode. These findings led Akira Yoshino, a Japanese scientist to find the prototype of the Lithium ion battery in 1985. More stable version of Lithium ion battery was commercialized in 1991 by Sony.

Introduction to Li as an Anode Material

Li is the lightest and most electro positive element. Li is a very prominent anode material, because batteries that compose of Li show high charge capacity (up to 750 mAh/g, 400 Wh/Kg and 500 Wh/l) [2]. Also Lithium is readily available and easy to handle in cells. These prominent characteristics of Li metal make Li as prominent materials in rechargeable batteries. However Li cells require significant amount of Li metal to gain a high capacity. This makes Li cells potentially unsafe. Lithiated Si or Sn nanostructures can be potential candidates to replace metallic Li. However, tin and silicon offer high

2

volumetric energy densities of 4347 Wh/l and 3914 Wh/l, but both of them suffer from high volume expansions (250% for tin and 400% for silicon).

Introduction to Sulfur as a Cathode Material

Sulfur has a theoretical charge capacity of 1672 mAh/g. That is five times higher than those of traditional transition metal oxides or phosphate. In addition to that Sulfur has other advantages such as low cost and environmental safeness. However Sulfur has its own drawbacks such as low electrical conductivity, dissolution of polysulfides in the electrolyte and volume expansion of Sulfur during discharge. These problems will lead to poor cycle life, low specific capacity and low energy efficiency. To overcome these problems with Sulfur, researches have intercalated Sulfur into conducting materials. Various carbon compounds such as Activated Carbon, Carbon Nanotubes or Mesoporous Carbon have been used to intercalate Sulfur. Reduced Graphene Oxide and Multiwall Carbon Nanotubes have proven to be promising material for intercalating Sulfur.

Introduction to Graphite Oxide

Graphene oxide has a history that extends many decades back. British chemist B.C. Brodie investigated the reactivity of flake graphite. He mixed potassium chlorate $KClO_3$ with slurry of graphite in fuming nitric acid HNO_3. Brodie determined that the resulting material was composed of Carbon, Hydrogen and Oxygen. After almost 60 years later, Staudenmaier, Hummers and Offeman developed an alternate oxidation method by reacting graphite with a mixture of potassium permanganate ($KMnO_4$) and concentrated sulfuric acid (H_2SO_4). Others have made GO by modified ways. But primary route of forming GO remains same. Many of the operative mechanisms, the precise chemical

structure models of GO proposed regular lattices composed of discrete repeat units. Hofmann and Holst's structure is composed of epoxy groups spread across the basal planes of graphite with a net formula of C_2O. Ruess's model also altered the basal plane structure to a sp^3 hybridized system rather than the sp^2 hybridized model. In 1969 Scholz and Boehm suggested a model that completely removed the epoxide and ether groups, substituting regular quinoidal species in a corrugated backbone. The most recent models of GO have rejected the lattice based model and have focused on a non-stoichiometric and amorphous alternative. Certainly the most well-known model is the one by Lerf and Klinowski (Figure 1.1.c). Anton Lerf and Jacek Klinowski have published several papers on the structure and hydration behavior of GO, and these are the most widely cited in the contemporary literature.

(a)

(b)

(c)
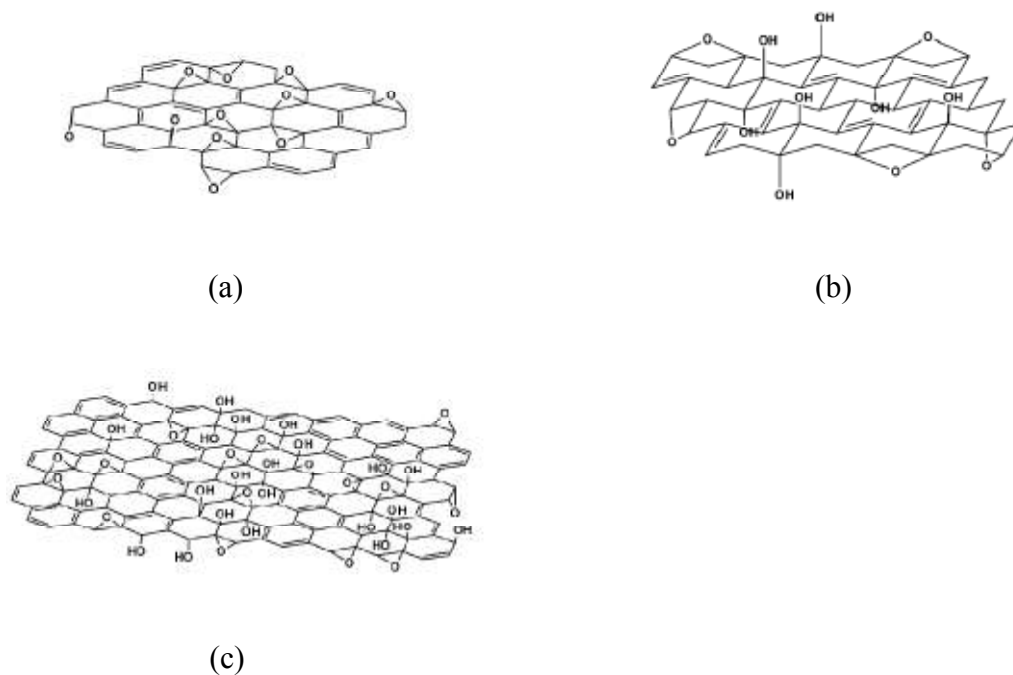
Figure 1.1: Models of Graphene Oxide (a) Hofmann model of GO (b) Ruess Model of GO (c) Lerf-Klinowski model of GO. Source: [3] Dreyer, D.R., et al.

4

Reduced Graphene Oxide

Graphene is a single layer of carbon atoms tightly packed into a two dimensional honeycomb sp^2 carbon lattice which shows many intriguing properties such as high thermal conductivity, superior mechanical and excellent electronic transport properties. These fascinating properties render Graphene suitable for many potential applications in nano-electronics, composite materials, sensors, batteries and super capacitors etc. Nevertheless, the realization of these applications is not feasible because the large-scale production of high quality Graphene via a simple low-cost method still remains a huge challenge. In recent years, various methods have been developed to prepare single or few-layer Graphene sheets. The first successful method was micro-mechanical exfoliation of bulk graphite. However, this method can only produce a very limited quantity of Graphene for fundamental research. Epitaxial growth of Graphene on metallic or metal Carbide substrates by chemical vapor deposition (CVD) of Hydrocarbons was attempted to produce Graphene [4]. But it needs ultrahigh vacuum or high temperature (1000 ^{O}C) environment and suffers from rather expensive templates, which is one of the biggest obstacles for the large-scale production of Graphene. Chemical synthesis through oxidation of Graphite provides an appealing alternative capable of large-scale production of Graphene [5]. Unfortunately the whole process is time-consuming which involves oxidation of graphite to graphite oxide, exfoliation to graphite oxide sheets and chemical reduction to Graphene. It inevitably leaves a large number of defects in Graphene. Thus a facile and practical strategy to produce high quality Graphene with high yield is urgently required. Recently, much attention has been paid to the production of large amounts of high-quality Graphene platelets which have attracted considerable attention for possible

applications in various fields. Chemical graphitization from Graphene Oxide (GO) to Graphene has been introduced for mass production. The use of the vapor phase is needed to pattern hydrophilic GOs on pre-patterned substrates, as well as in situ reduction to hydrophobic reduced graphene oxides (RGOs). Moreover, a low-temperature process below the glass transition temperature is essential for flexible device fabrication on plastic substrates. Until now, the chemical reduction of GO has entailed the use of hydrogen sulphide, hydrazine, $NaBH_4$, Dimethylhydrazine and hydroquinone. Such reduction reagents have been reported to achieve a high degree of GO reduction in the solution phase. Recently, electrochemical reduction methods have been introduced without the use of reducing reagents.

Carbon Nanotubes and Multiwall Carbon Nanotubes

Since the discovery of Carbon Nanotubes (CNTs), they have been very useful in the field of nanotechnology due their unique structural integrity. CNTs have high conductivity and high aspect ratio which help them to form a network of tubes. In addition they perform high stiffness, strength. CNTs transfer their mechanical load to the polymer matrix at a much lower weight percentage than carbon or carbon fiber. Their attractive electronic and mechanical properties can be used in numerous applications, such as field emission displays, nano composite materials, nano sensors and logic elements. Singled Walled Carbon Nanotubes (SWNTs) are special type of CNTs which consist only one layer of Graphene. Multiwall Crbon Nanotubes (MWCNTs) compose of multiple rolled layers of Graphene. MWCNTs are not clearly defined due to their complexity. However MWCNTs exhibits advantage over SWCNTs, such as ease of mass production, low product cost per unit and enhanced chemical and thermal stability.

ELECTROCHEMICAL PRINCIPLES AND REACTIONS

Theoretical Cell Voltage/Capacity and Energy

The theoretical voltage and capacity of a cell are a function of the anode and cathode materials. In this section it is objected to describe the important parameters of batteries.

Free Energy

Gibbs free energy represents the usable energy from a given chemical reaction. Whenever a reaction occurs, there is a decrease in the free energy of the system, which is expressed as

$$G_o = -nFE_o$$

where, F: Constant known as Faraday (96,500 C or 26.8 Ah), n: Number of electrons involved in stoichiometric reaction and E_o: Standard potential measured in Volts

Theoretical Voltage/Potential

The standard potential of the cell can be calculated from free-energy data or obtained experimentally. A listing of electrode potentials (reduction potentials) under standard conditions is given in Table 1.1.a and 1.1.b. An example of calculating the standard potential of a cell is shown in the following example. Normally the oxidation potential is the negative value of the reduction potential

 Anode (oxidation potential) + Cathode (reduction potential) = Standard cell potential

For example, in the reaction $ZnCl_2 \rightarrow Zn^{+2} + 2Cl^-$

$$Zn \rightarrow Zn^{+2} + 2e \ (0.76 \ V)$$

$$2Cl + 2e \rightarrow 2Cl^- \ (1.36 \ V)$$
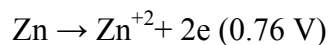
$$E = 0.76 \ V + 1.36 \ V = 2.12 \ V$$

The cell voltage is also dependent on other factors including concentration and temperature as expressed by the Nernst equation. For example; for a reaction a → b

$$E = E^0 - \frac{RT}{nF} ln \frac{a_b}{a_a}$$

where, a_i: activity of relevant species, R: gas constant and T: absolute temperature

Theoretical Capacity (Coulombic)

The theoretical capacity of a cell is determined by the amount of active materials in the cell. Total quantity of charge involved in the electrochemical reaction is defined in terms of coulombs or ampere-hours which is directly associated with the quantity of charge obtained from the active materials. Theoretically one gram-equivalent weight of a material will deliver 96,487 C or 26.8 Ah. The electrochemical equivalence of typical materials is listed in table 1.1.a and 1.1.b. The theoretical charge capacity of an electrochemical cell based only on the active materials participating in the electrochemical reaction is calculated from the equivalent weight of the reactants.

The theoretical voltages and capacities of a number of the major electrochemical systems are given in table 1.2. These theoretical values are based on the active anode and cathode materials only. Water, electrolyte or any other materials that may be involved in the cell reaction are not included in the calculation.

8

Material	Atomic/ Molecular weight	Standard reduction potential at 25°C, V	Valance Change	Melting point, °C	Density g/cm³	Capacity Ah/g
H_2	2.01	0	2	-	-	26.59
Li	6.94	-3.01	1	180	0.54	3.86
Na	23.0	-2.71	1	98	0.97	1.16
Mg	24.3	-2.38	2	650	1.74	2.20
Al	26.9	-1.66	3	659	2.69	2.98
Ca	40.1	-2.84	2	851	1.54	1.34
Fe	55.8	-0.44	2	1528	7.85	0.96
Zn	65.4	-0.76	2	419	7.14	0.82
Cd	112.4	-0.40	2	321	8.65	0.48
Pd	207.2	-0.13	2	327	11.34	0.26

Source: Hand book of batteries by David Linden, Thomas B Reddy [2]

Table 1.1.a: Anode material properties

Material	Atomic/ Molecular weight	Standard reduction potential at 25°C, V	Valance Change	Melting point, °C	Density g/cm³	Capacity Ah/g
S	32	-0.48	2	115	2.07	.167
MnO_2	86.9	1.28	1	-	5.0	0.308
FeS_2	119.9	-	2	-	-	0.89

Source: Hand book of batteries by David Linden, Thomas B Reddy [2]

Table 1.1.b: Cathode material properties

Battery type	Anode	Cathode	Reaction Mechanism	Theoretical Values	
				V	mAh/g
Leclanche	Zn	MnO_2	$Zn+2MnO_2 \rightarrow ZnO+Mn_2O_3$	1.6	224
Magnesium	Mg	MnO_2	$Mg+2MnO_2+H_2O \rightarrow Mn_2O_3+Mg(OH)_2$	2.8	271
AlkalineMnO$_2$	Zn	MnO_2	$Zn+2MnO_2 \rightarrow ZnO+Mn_2O_3$	1.5	224
Mercury	Zn	HgO	$Zn+HgO \rightarrow ZnO+Hg$	1.34	190
Mercad	Cd	HgO	$Cd+HgO+H_2O \rightarrow Cd(OH)_2+Hg$	0.94	163
Silver Oxide	Zn	Ag_2O	$Zn+Ag_2O+H_2O \rightarrow Zn(OH)_{2+}2Ag$	1.6	180
Zinc/O$_2$	Zn	O_2	$Zn+1/2O_2 \rightarrow ZnO$	1.65	658
Zinc/air	Zn	air	$Zn+1/2O_2 \rightarrow ZnO$	1.65	820
Li/SOCl$_2$	Li	$SOCl_2$	$4Li+2SOCl_2 \rightarrow 4LiCl+S+SO_2$	3.65	403
Li/SO$_2$	Li	SO_2	$2Li+2SO_2 \rightarrow Li_2S_2O_4$	3.1	379
LiMnO$_2$	Li	MnO_2	$Li+MnO_2 \rightarrow MnO_2(Li^+)$	3.5	286
Li/FeS$_2$	Li	FeS_2	$4Li+FeS_2 \rightarrow 2Li_2S+Fe$	1.8	726
Li/(CF)$_n$	Li	$(CF)_n$	$nLi+(CF)_n \rightarrow nLiF+Nc$	3.1	706
Li/I$_2$	Li	I_2	$Li+1/2I_2 \rightarrow LiI$	2.8	200
Li/S	Li	S	$2Li+S \rightarrow Li_2S$	2.53	1672

Source: Hand book of batteries by David Linden, Thomas B Reddy [2]

Table 1.2: Theoretical capacity and voltage of major battery systems

Theoretical Energy

The capacity of a cell can also be considered as energy (watt-hour) basis by taking both the voltage and the quantity of electricity into consideration. This theoretical energy value is the maximum value that can be delivered by a specific electrochemical system:

Watt-hour (Wh) =voltage (V) * ampere-hour (Ah)

Batteries are electrochemical devices which convert chemical energy into electrical energy by electrochemical oxidation and reduction reactions, which occur at the electrodes. A typical cell consists of an anode where oxidation takes place during discharge, a cathode where reduction takes place and an electrolyte which conducts the

ions within the cell. The maximum electric energy that can be delivered by the chemicals that are stored within or supplied to the electrodes in the cell depends on the change in free energy G of the electrochemical couple. Not all the energy is given out during the discharge. Losses due to polarization occur when a load current i pass through the electrodes. These losses include: (1) activation polarization which drives the electrochemical reaction at the electrode surface and (2) concentration polarization which arises from the concentration differences of the reactants and products at the electrode surface and in the bulk as a result of mass transfer. These polarization effects consume part of the energy giving waste heat.

Most cell electrodes are composite bodies made of active material, binder, performance enhancing additives and conductive filler. They usually have a porous structure of finite thickness. Another important factor that strongly affects the performance or rate capability of a cell is the internal impedance of the cell. It causes a voltage drop during operation consuming part of the useful energy as waste heat. This voltage drop is usually referred to as ''ohmic polarization'' or IR. The total internal impedance of a cell is the sum of the ionic resistance of the electrolyte (within the separator and the porous electrodes), the electronic resistances of the active mass, the current collectors and electrical tabs of both electrodes and the contact resistance between the active mass and the current collector. These resistances are Ohmic in nature.

When connected to an external load R, the cell voltage E can be expressed as in [2]

$$E = E_o - \{(\eta_{ct})_\alpha + (\eta_c)_\alpha\} - \{(\eta_{ct})_c + (\eta_c)_c\} - iR_i = iR$$

where, E_0: electromotive force or open-circuit voltage of cell, $(\eta_{ct})_a, (\eta_{ct})_c$: activation polarization or charge-transfer overvoltage at anode and cathode, $(\eta_c)_a, (\eta_c)_c$: concentration polarization at anode and cathode, i: operating current of cell load and R_i: internal resistance of cell

As shown in above equation, the useful voltage delivered by the cell is diminished by polarization and the internal IR drop. Figure 1.2 shows the relation between cell polarization and discharge current.
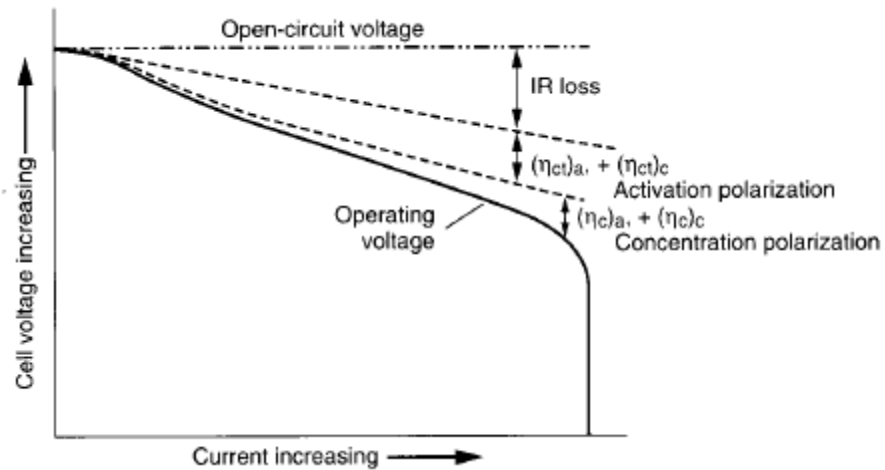
Figure 1.2: Polarization effect of a cell. (Source: Hand book of batteries by David

         Linden, Thomas B Reddy [2])

There are many factors which affect the magnitude of the charge-transfer reaction, diffusion rates, and magnitude of the energy loss. These factors include electrode formulation and design, electrolyte conductivity, and nature of the separators. There exist some essential rules, based on the electrochemical principles which are important in the design of batteries and fuel cells to achieve a high operating efficiency with minimal loss of energy.

1. The conductivity of the electrolyte should be high enough that the IR polarization is not excessively large for practical operation. A cell may be designed to have improved rate capability, with a higher electrode interfacial area and thin separator to reduce the IR drop due to electrolyte resistance.

2. Chemical stability of electrolyte with the electrodes is very important.

3. The rate of electrode reaction at both the anode and the cathode should be sufficiently fast so that the activation or charge-transfer polarization is not too high to make the cell inoperable. Using a porous electrode can minimize this factor.

4. The cell should have adequate electrolyte transport to facilitate the mass transfer to avoid building up excessive concentration polarization. Proper porosity and pore size of the electrode, adequate thickness and structure of the separator, and sufficient concentration of the reactants in the electrolyte are very important to ensure functionality of the cell

5. The material of the current collector or substrate should be compatible with the electrode material and the electrolyte without causing corrosion problems. The design of the current collector should provide a uniform current distribution and low contact resistance to minimize electrode polarization during operation.

ELECTROANALYTICAL TECHNIQUES

Cyclic Voltammetry

Cyclic Voltammetry (or linear sweep voltammetry as it is sometimes known) is probably one of the more versatile techniques available to the electrochemist.

This technique uses a linearly changing voltage (ramp voltage) to an electrode. The scan of voltage might be 2 V from an appropriate rest potential such that most electrode reactions would occur. Commercially available instrumentation provides voltage scans as wide as 5 V. To describe the principles behind cyclic voltammetry, a model chemical equation can be used which describes the reversible reduction of an oxidized species O,

$$O + ne \leftrightarrow R$$

In cyclic voltammetry, the initial potential sweep is represented by

$$E = E_i - vt$$

Where, E_i: initial potential, t: time and v: rate of potential change or sweep rate (V/ s)

The reverse sweep of the cycle is defined by

$$E = E_i - v't$$

Where v' is often the same value as v. When the applied voltage approaches that of the reversible potential for the electrode process, small current flows. The "true" electrode potential is modified by the capacitance effect as it is also by the Ohmic resistance of the solution. The corrected equation will be as follows;

$$E = E_i - vt + r(i_f + i_c)$$

where r; cell resistance, i_f: faradic current and i_c: capacity current

At small values of voltage sweep rate, typically below 1 mV/ s, the capacity effects are small and in most cases can be ignored. At greater values of sweep rate, a correction needs to be applied to interpretations of i_p.

Cyclic voltammetry provides both qualitative and quantitative information on electrode processes. A reversible, diffusion-controlled reaction exhibits an approximately symmetrical pair of current peaks, as shown in figure 1.3. The voltage separation ΔE of these peaks is

$$\Delta E = \frac{2.3RT}{nF}$$

 The value ΔE of is independent of the voltage sweep rate.

The current peaks are more separated and the shape of the peak is less sharp at its summit and is generally more rounded for a quasi-reversible processes figure 1.4). The voltage of the current peak is dependent on the voltage sweep rate and the voltage separation is much greater.
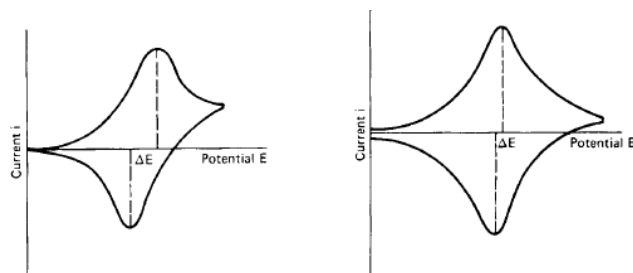
Figure 1.3: Cyclic Voltammetry of a reversible, diffusion-controlled reaction. (Source:

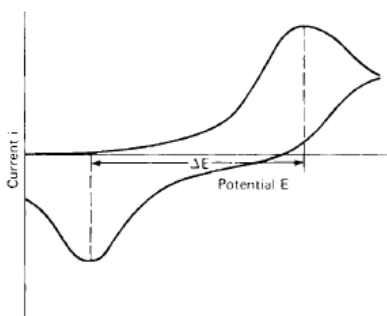Hand book of batteries by David Linden, Thomas B Reddy [2])

Figure 1.4: Cyclic Voltammetry of a quasi-reversible processes.(Source: Hand book of

batteries by David Linden, Thomas B Reddy [2])

FACTORS AFFECTING BATTERY PERFORMANCE

Capacity, energy output and performance of a battery are among the many factors influence the operational characteristics. It should be noted that because of the many possible interactions, these effects can be presented only as generalizations and that the influence of each factor is usually greater under the more strict operating conditions. For example, the effect of storage is more pronounced not only with high storage temperatures and long storage periods, but also under more severe conditions of discharge following storage. After a given storage period, the observed loss of capacity (compared with a fresh battery) will usually be greater under heavy discharge loads than

16

under light discharge loads. Similarly, the observed loss of capacity at low temperatures (compared with normal temperature discharges) will be greater at heavy than at light or moderate discharge loads. Furthermore it should be noted that even within a given cell or battery design, there will be performance differences from manufacturer to manufacturer.

Different References Made to the Voltage of a Cell or Battery

1. The theoretical voltage is a function of the anode and cathode materials, the composition of the electrolyte and the temperature (usually stated at 25C).

2. The open-circuit voltage is the voltage under a no-load condition and is usually a close approximation of the theoretical voltage.

3. The closed-circuit voltage is the voltage under a load condition.

4. The nominal voltage is one that is generally accepted as typical of the operating voltage of the battery as, for example, 1.5 V for a zinc-manganese dioxide battery.

5. The working voltage is more representative of the actual operating voltage of the battery under load and will be lower than the open-circuit voltage.

6. The average voltage is the voltage averaged during the discharge.

7. The midpoint voltage is the central voltage during the discharge of the cell or battery.

8. The end or cut-off voltage is designated as the end of the discharge. Usually it is the voltage above which most of the capacity of the cell or battery has been delivered.

The voltage difference caused by IR losses due to cell (and battery) resistance and polarization of the active materials during discharge is illustrated in figure 1.5. In an ideal

case, the discharge of the battery proceeds at the theoretical voltage until the active

materials are consumed and the capacity is fully utilized. The voltage then drops to zero.

Under real conditions, the discharge curve is similar to the other curves in figure 1.5. The

initial voltage of the cell under a discharge load is lower than the theoretical value due to

the internal cell resistance and the resultant IR drop as well as polarization effects at both

electrodes. The voltage also drops during discharge as the cell resistance increases due to

the accumulation of discharge products, activation and concentration, polarization and

related factors. Curve 2 represents a cell with a higher internal resistance or a higher

discharge rate, or both compared to the cell represented by curve 1. As the cell resistance

or the discharge current is increased, the discharge voltage decreases and the discharge
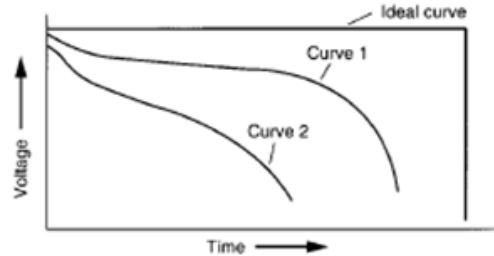
shows a more sloping profile

Figure 1.5: Deviation of theoretical voltage due to IR drop. (Source: Hand book of

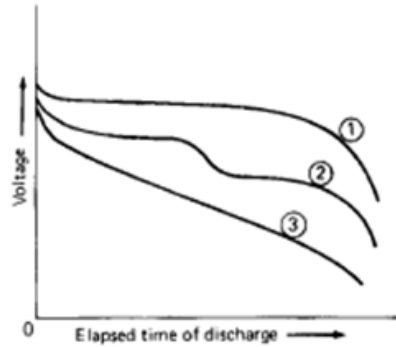batteries by David Linden, Thomas B Reddy [2])

Figure 1.6: Battery discharge voltage profiles. (Source: Hand book of batteries by David

Linden, Thomas B Reddy [2])

The specific energy that is delivered by a battery in practice is lower than the theoretical

specific energy of its active materials due to:

1. The average voltage during the discharge is lower than the theoretical voltage.

2. The battery is not discharged to zero volts and all of the available ampere-hour

capacity is not utilized.

The delivered specific energy is lower than the theoretical energy. The shape of the

discharge curve can vary depending on the electrochemical system, cell design and other

discharge conditions. Typical discharge curves are shown in figure 1.6. The flat discharge

(curve 1) is representative of a discharge where the effect of change in reactants and

reaction products is minimal until the active materials are nearly exhausted. The plateau

profile (curve 2) is representative of two-step discharge indicating a change in the

reaction mechanism and potential of the active material(s). The sloping discharge (curve

3) is typical when the composition of the active materials, reactants, internal resistance,

and so on, changes during the discharge, affecting the shape of the discharge curve similarly.

CHAPTER 2

METHODOLOGY

Due to the poor conductivity and production of intermediate polysulfides, fabricating a Sulfur cathode with good cycle life with the practical capacity close to 1500 mAh/g at least for 100 cycles have been always challenging. In previous work [1], coating of Sulfur with conducting surfactant such as Triton X-100, has shown a somewhat promising result, yet it too tends shows capacity fade over 100 cycles. This surfactant coating method has been tested in different ways [6]. But in this research work, a novel technique has been tested to overcome the problems such as capacity fading over higher number of cycles and efforts were taken to achieve 1000 mAh/g over 50 cycles.

In this research, a novel cathode material was designed to host sulfur using Reduced Graphene Oxide and activated Multiwall Carbon Nanotubes. In contrast from the previous works [1, 6, 7], here the sulfur source is Organo Sulfides such as Phenyl Disulfide, Dibenzyl Disulfide and DibenzylTrisulfide. The potential use of Phenyl Disulfide as a cathode material on a copper sheet has been demonstrated before [8]. When the Organo Sulfide compound with aromatic rings attached is used in RGO, it gives extra benefits on anchoring Sulfur atoms in Carbon Structure. Because, according to the figure 2.1, RGO has a planner honeycomb structure with vacant sp^2 hybridized orbital perpendicular to the planer structure. Similarly said Organo Sulfides with bulk

aromatic rings attached have sp^2 hybridized orbitals perpendicular to the aromatic ring and they will undergo π bonds with planner structure. It is obvious that that the RGO planes will be in different orientations. But the twisted nature of the bulk aromatic rings that resides both sides of the sulfur atoms can make parallel bonds with randomly oriented RGO very well.
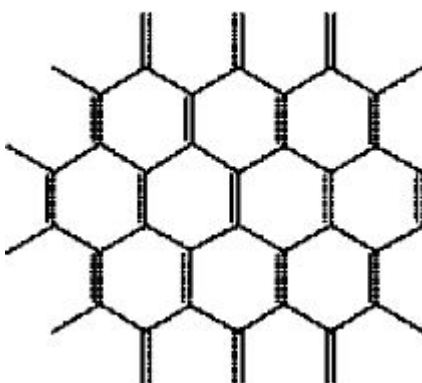

Figure 2.1: Two dimensional structure of Reduced Graphene Oxide

Having set the RGO structure to bond well with Phenyl Disulfide, Benzyl Disulfide or Benzyl Trisulfide, the next objective is to make channels to propagate Li$^+$ ions into the cathode material. By synthesizing channels inside the cathode material, it is expected to let most of the Sulfur content to react with Li$^+$. At the same time channel structure will improve the cell performance when the cell is charged and discharged. The said channel structure is synthesized using activated Multiwall Carbon Nanotubes.

When the Phenyl Disulfide or Dibenzyl Disulfide is used, it must be melted with an appropriate amount of Sulfur powder and then the both the materials must be quickly cooled down. By doing so, polysulfur chain will be attached in between two Phenyl

groups or two Benzyl groups. Table 2.1 shows the bonding energy of intermediate S—S is weak compared to the Ph—S or Ph-CH$_2$-S. According to the data given in the table 2.1, when Li$^+$ attaches, it is most likely that the Li $^+$ makes bonds with intermediate Sulfur atoms forming Li$_2$S. When the intermediate Sulfur is released, Ph—S or Ph-CH$_2$-S become stabilized by the resonance bond effect [9] between Sulfur and Ph group or Ph-CH$_2$ group. This resonance nature is due to the electro-philic nature of the Ph group and Ph-CH$_2$ group. Hence this gives an advantage of stabilizing the Ph—S or Ph-CH$_2$-S when the cell is in operation.

Compound	Dissociation energy (Kcal/mol)
CH$_3$S-SCH$_3$	73
CH$_3$S-SC$_2$H$_5$	72
C$_2$H$_5$S-SC$_2$H$_5$	70
PhCH$_5$S-SCH$_5$Ph	26-32
S$_8$	26-32

Source: Organic Sulfur chemistry: structures and mechanism, Shigeru Oae [9]

Table 2.1: Selected bond dissociation energies of S-S linkages

CHAPTER 3

MATERIAL SYNTHESIS AND CELL FABRICATION

Synthesis of Reduced Graphene Oxide

Hummer's Method was used to synthesis Graphene Oxide from graphite. The procedure is as follows. First 1 g of Graphite powder and 23 ml of concentrated H_2SO_4 were put into a round bottom flask with a magnetic stirrer inside and kept it at $-20\ ^oC$ for 24 h. A refluxing column was attached to the round bottom flask and water was supplied to the refluxing column and then the round bottom flask was kept in an ice bath. After that 3 g of $KMnO_4$ was slowly added while the mixture was stirring. After the $KMnO_4$ was completely dissolved, temperature was slowly increased to 40 ^oC and kept it there for 30 minutes while stirring. Then 46 ml of water is added slowly and temperature was raised to 90 ^oC and kept there for 15 minutes and then 140 ml of distilled water and 10 ml of 30 % H_2O_2 was added. Then the Graphene Oxide product was extracted by centrifuging three times at 7500 rpm for 10 minutes with water and then with acetone at 7500 rpm for 10 minutes.

Synthesis of Reduced Grahene Oxide from Graphene Oxide

300 mg of Graphene Oxide was mixed with 30 ml of distilled water. Then 1.92 ml of Hydrazine was added and sonicated for 5 minutes. Then the GO suspension was sealed in

an autoclave and kept at 100 $^{\circ}$C for 12 hours. Then the material was washed with water until the PH become 7 then extracted by centrifuging.

$$2GO + N_2H_4 \rightarrow 2.Graphene + 2H_2O + N_2$$
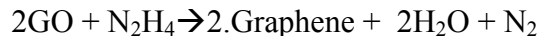
Activation of Multiwall Carbon Nanotubes

Following the previously done work [10] 1.5 mg of Multiwall Carbon Nanotubes were mixed with KOH platelets in such a way that KOH/MWCNT mass ratio of 7:1 in 20 ml alcohol-water (v/v=1:1). After drying at 110 $^{\circ}$C for 12 hours the activation process was carried out at 800 $^{\circ}$C for 1 hour at a heating rate of 5 $^{\circ}$C/min under N_2 flow 5 ml/s. The sample was then washed with 1.0 moldm^{-3}HCl for 2 hours and filtered. Finally the sample was dried at 100 $^{\circ}$C.
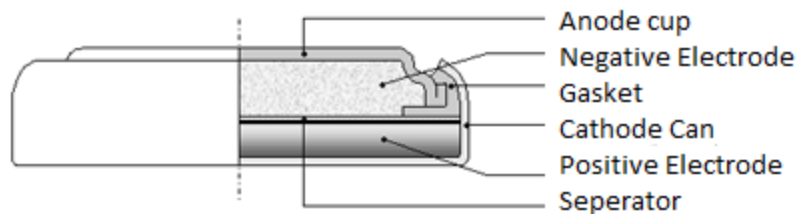
Cell Assembly

Figure 3.1: Cross section of a coin/button cell

In this research the button cell (figure 3.1) type was always used to assemble the cell components together. A typical cell is composed of an outer casing made with stainless steel. In fact the outer casing comes with two separate parts as cathode and anode. The anode has a plastic insulator around it to prevent short circuiting and to make good sealing when the cell is made. The current collector is a round shape stainless steel

component that establishes good conductivity between cathode and the outer casing. In addition to that there is a spring in between the current collector and the outer casing to prevent any loose connection that can occur when the cell is made. The main components of a cell, Anode, Cathode, Separator and the Electrolyte are discussed herein. First the lithium foil that has a thickness of about 0.5 mm is cut into circular shape in such a way that it loosely fits in the anode side of the stainless steel case. Then a separator made of glass and ceramic was used to physically separate the anode and the cathode. The electrolyte was synthesized according to previously published work [1] and only 0.1 ml was used in cell assembling.

Different methods have been tested starting from simple mechanical mixing of Sulfur in Carbon material. Then efforts were taken to synthesize a novel material for Sulfur Cathode. However the main focus is to design a stable cathode with Sulfur as the active material. All methods have been summarized herewith.

Method 1

5 mg of Sulfur powder was mechanically mixed with 10 mg of RGO or Multiwall Carbon Nanotubes. As a binder 5 mg Toluene Acetylene Black was used. Then cells were assembled using the electrolyte described in [1]; 1.0M lithium bis-trifluoromethanesulfonylimide in 1,3-dioxolane and 1,2-dimethoxyethane (volume ratio 1:1).

Method 2

96 mg of sulfur was dispersed in 20 ml of 0.1 M Na_2S and sonicated for 30 minutes. Then a Polysulfide aqueous solution was formed by heating the above solution in 60^oC water

bath. 180 mg of GO was dispersed in 10 ml of distilled water and sonicated. Then the GO suspension was added into a 20 ml of $FeCl_3$ solution and stirred for 10 min. Then prepared polysulfide aqueous solution was added in the $FeCl_3$ + GO suspension and reacted for another 60 ^{o}C. Finally the product was washed with HCl and vacuum dried.

In this method Sulfur was intercalated in the RGO layers while the GO is reduced. Cells were assembled using 10 mg of functionalized RGO with Sulfur and 5 mg of Toluene Acetylene Black binder. The 0.1 ml of electrolyte used is the one which discussed in [1].

Method 3

Previously done work [1] was followed for Sulfur encapsulating. 0.098 g of $Na_2S_2O_3$ was mixed with 0.1 ml of HCl. This mixture was stirred in a 5 ml of Triton X-100 for about 15 min at 50 ^{o}C. Then 50 mg of RGO and 50 mg of Carbon black was mixed and stirred. After that the product was dried at 60 ^{o}C for 24 hrs.

Then the cells were assembled using 20 mg of the product with 5 mg of Toluene Acetylene black. 0.1 ml of electrolyte was used.

Method 4

Organo Sulfur compounds were used as the sulfur source in the cell. Phenyl Disulfide and Dibenzyl Disulfide were used as Organo Sulfide compound. 5 mg of Sulfur powder is mechanically mixed with 20 mg of either of Organo Sulfur compounds and heat treated at 130 ^{o}C to just melt down the both materials. In a separate vessel, 10 mg of Reduced Graphene Oxide and 10 mg of activated Multiwall Carbon Nanotubes were mixed mechanically. Then the both the mixtures were mixed together until they become a fine

powder like mixture. Then the mixture is put on to a stainless steel mesh and pressed under 1 ton force using a mechanical pressing device.After that the electrode was heat treated 120°C.

Method 5

After the experimented results of method 4, it was concluded that Dibezyl Tri-sulfide is more beneficial than Dybenzyl Disulfide since DibenzylTrisulfide has middle Sulfur which can participate to produce full capacity in a Li-S cell. However unlike the Dybenzyl Disulfide, DybenzylTrisulfide is not abundantly commercially available or they are very expensive. Yet various forms of organo tri-silfide can be found in natural sources such as onion [11, 12]. In this research DybenzylTrisulfide was synthesized by following method.

First N,N′-Thiobisphthalamide was synthesized by following the previous work [13]. According to that Sulfur Monochloride was added drop wise to 1 g of Phthalamide. The mixture was stirred in a cocked conical flask for 20 hours at 28 °C. A yellow color product was isolated by filtration. The reaction is as follows.
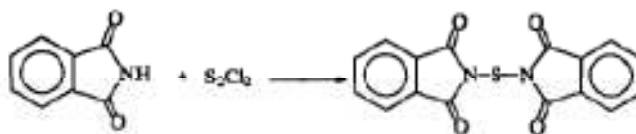
Then previously done work [11] was referred on synthesizing DibenzylTrisulfide. The procedure is as follows. 065 g of N,N′-Thiobisphthalamide and 0.50 g α-Toluenethiol are dissolved in 50 ml of Benzene. The reaction was refluxed for 24 hours while mixing. After that white precipitate was collected by filtering. Then benzene was evaporated from

the filtrate and needle like pale yellow DibenzylTrisulfide was noted. The product was analyzed under NMR for confirmation of the product. According to NMR spectrum (figure 3.2) the existence of Benzyl group was confirmed. But to further confirmation of Trisulfide group, Mass spectroscopy was needed.
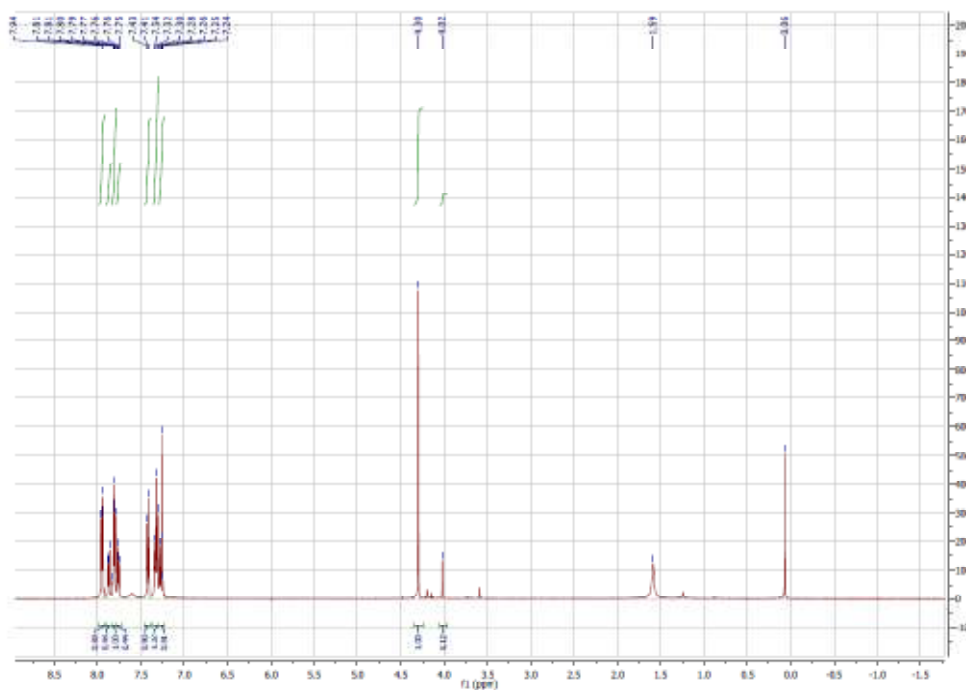

Figure 3.2: NMR spectrum of DiBenzyl Trisulfide

CHAPTER 4

RESULTS AND CONCLUSIONS

In this chapter, the material characterization by Raman Spectrum Analysis and SEM techniques are discussed. The electrochemical properties of the cell were studied using Cyclic Voltammetry. Cell capacity and the cell performances upon discharging and charging was measured using Arbin 2000 battery tester (Figure 4.2).

Figure 4.1: Stages of a coin cell
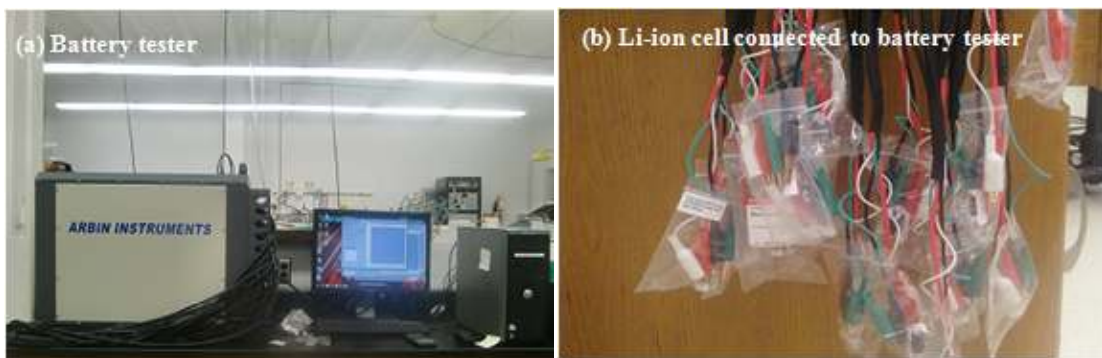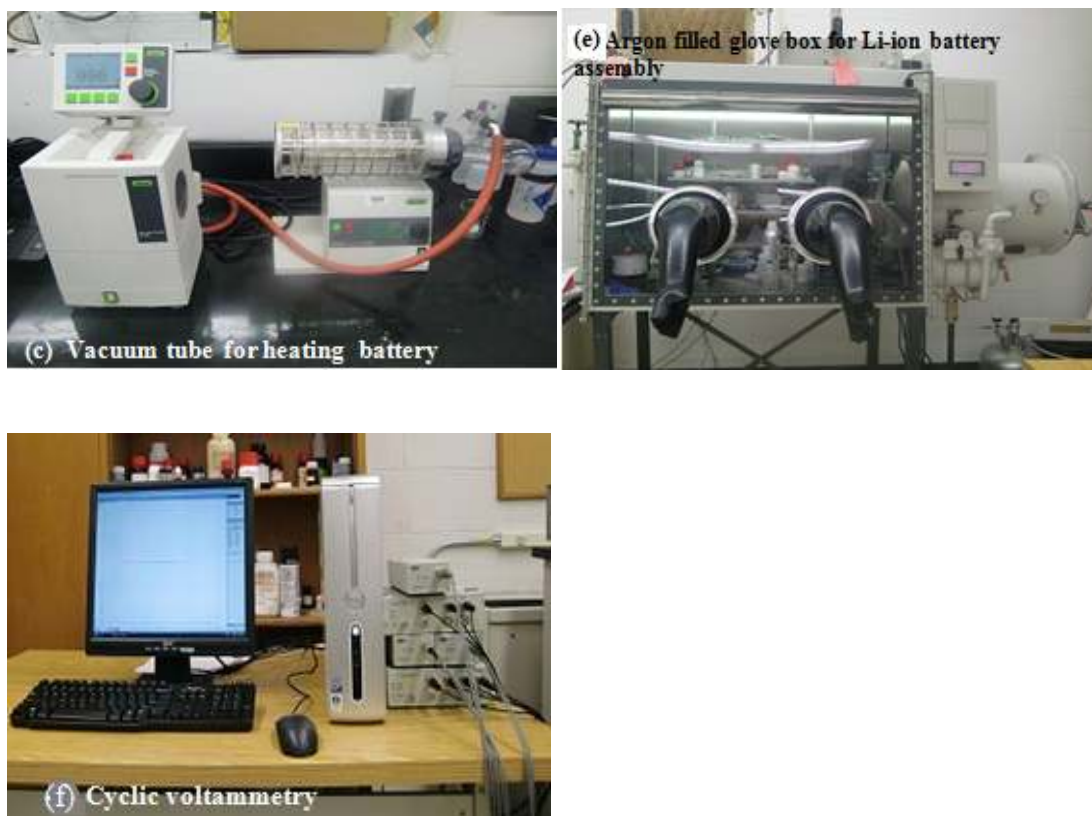
Figure 4.2: Laboratory equipments of battery testing and assembling

Raman Characterizing of RGO

Raman spectra of RGO on a glass substrate was measured and compared with respect to the Raman spectrum of Graphite.
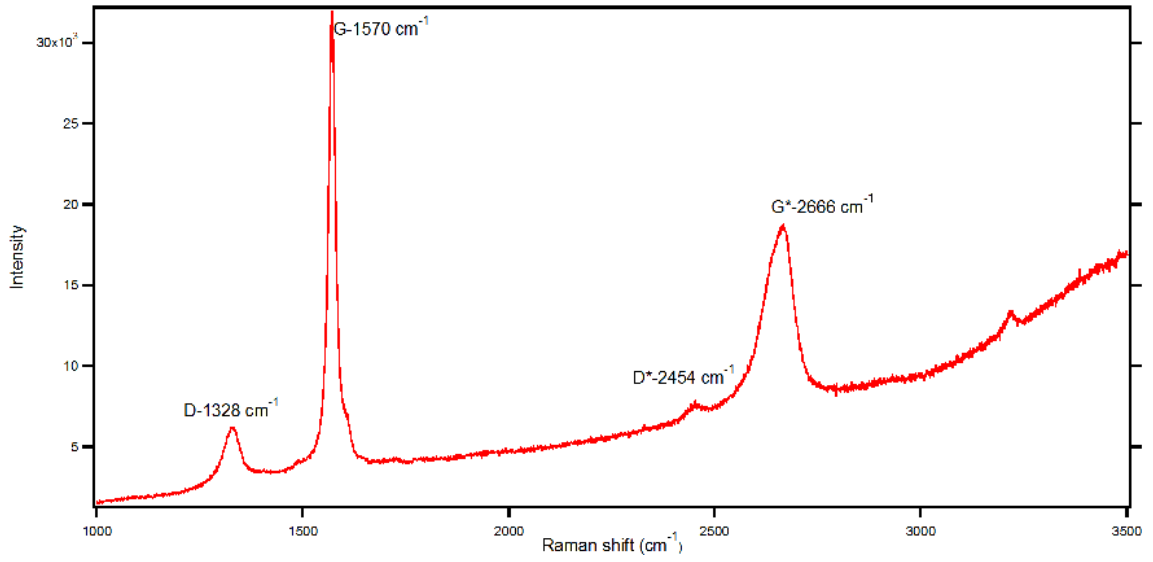
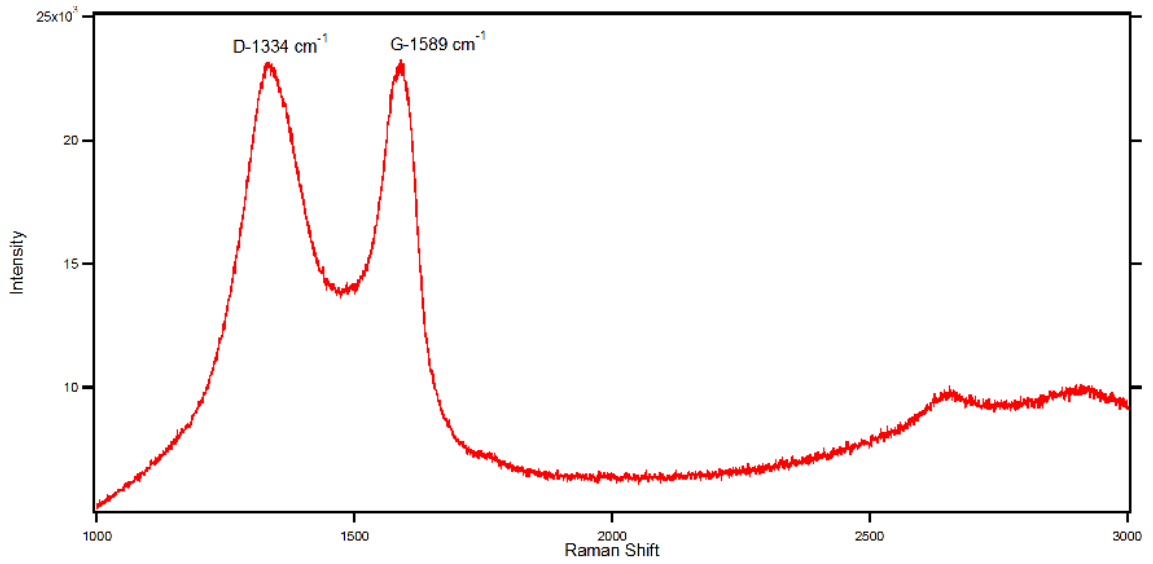Figure 5.1: Raman spectrum of Graphite
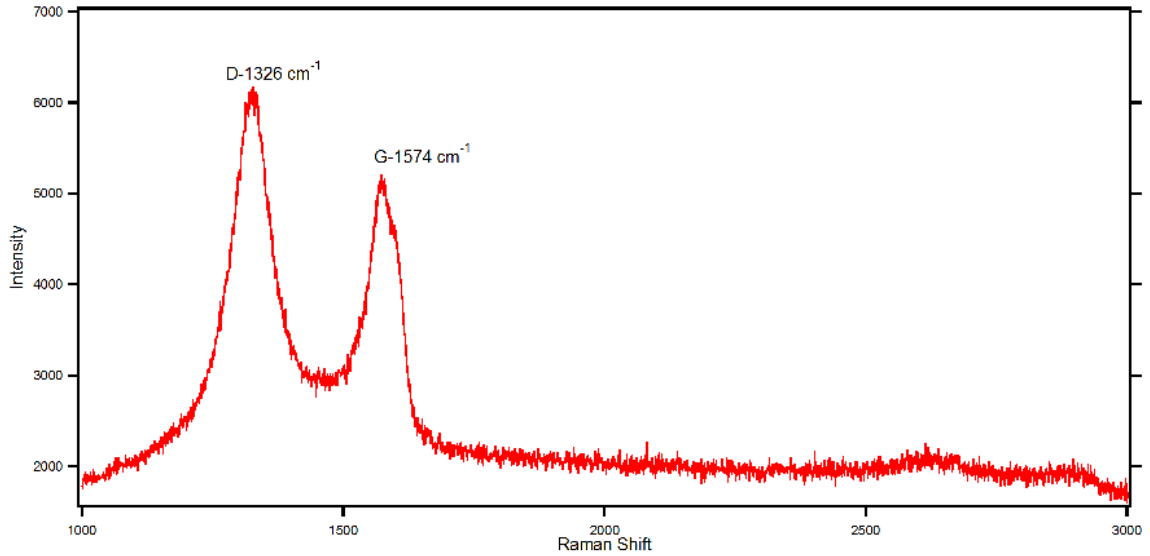

Figure 5.2: Raman spectrum of Graphene Oxide

Figure 5.3: Raman spectrum of Reduced Graphene Oxide

Differences between Raman peaks of Graphite, Graphene Oxide and RGO are evident as shown in figures 5.1, 5.2, and 5.3. The characteristic feature of Graphite to Graphene Oxide is the D and G bands. In the Raman spectroscopy of Graphene Oxide, both D and G bands have almost the same peak intensities. However the intensity of the G band of Graphene Oxide becomes lower when it transforms to Reduced Graphene Oxide as shown in figure 5.3.
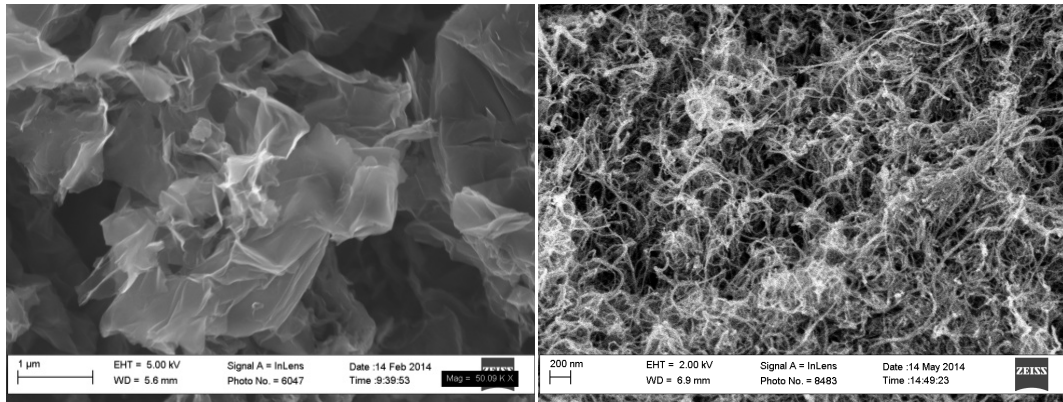
(a)   (b)

Figure 5.4: SEM images of synthesized material (a) SEM image of Reduced Graphene

Oxide reduced by Hydrazine, (b) SEM image of Activated MWCNT

It was observed that RGO reduction done by the Hydrazine is very effective. The two

dimensional layers are clearly visible in SEM image 5.4.a. The activated Multiwall

Carbon Nanotubes was analyzed under SEM. Also the synthesized material was analyzed

under SEM after the RGO and Multiwall Carbon Nanotubes were mixed to 50: 50 ratio.
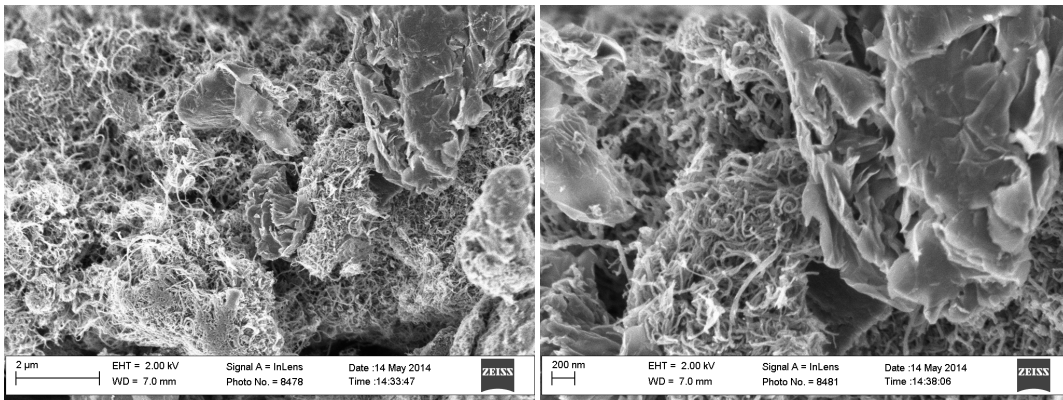

(a)   (b)

Figure 5.5: SEM images of RGO: Activated Multiwall Carbon Nanotubes 50:50 ratio

mixture (a) and (b) are the same material with different magnifications

34

SEM images in figures 5.5.a and 5.5.b depict how the RGO layers reside in Activated MWCNT. These SEM images reveal the channeled structure and two dimensional RGO layer structure to support the bonds between bulk aromatic structure of Phenyl Disulfide or Dibenzyl Disulfide or Dibenzyl TriSulfide. This RGO@MWCNT is coated by Dibenzyl Disulfide or Dibenzyl Trisulfide. The coating of such polysulfide is visible in SEM images in figure 5.6.
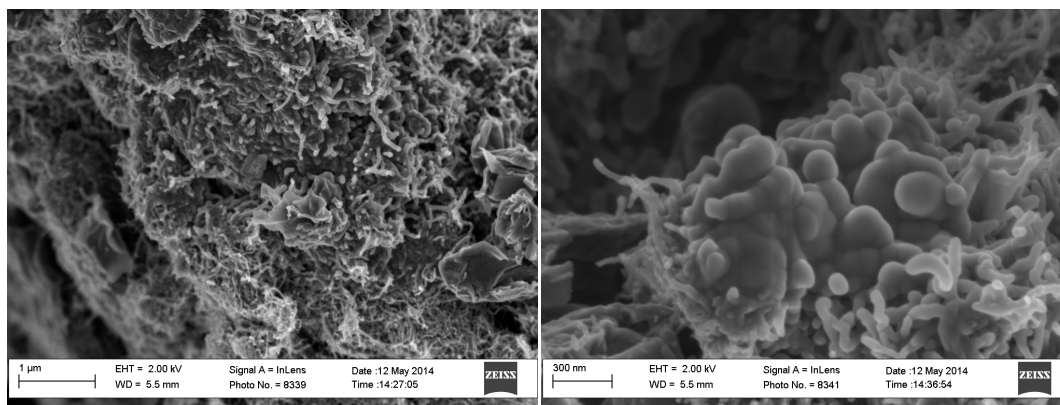

(a)   (b)

Figure 5.6: SEM images of Dibenzyl Disulfide treated RGO@MWCNT

However Dybenzyle Disulfide coated RGO@MWCNT is not important. Because Li^+ will be linked to $Ph-CH_2-S-$ by breaking the S-S bond. That means the cell will give only half the theoretical capacity since Sulfur only contributes one electron. Therefore intermediate Sulfur atom is a necessity to achieve the full capacity. To synthesize such a material, method 4 was followed and analyzed under SEM. In figure 5.7.a and 5.7.b Sulfur particles are visible as white dots. But in figure 5.8.a and 5.8.b the sulfur particles are not visible since the Sulfur and the Organo Sulfur compounds melts and upon cooling they form Organo Polysulfides in RGO@MWCNT structure
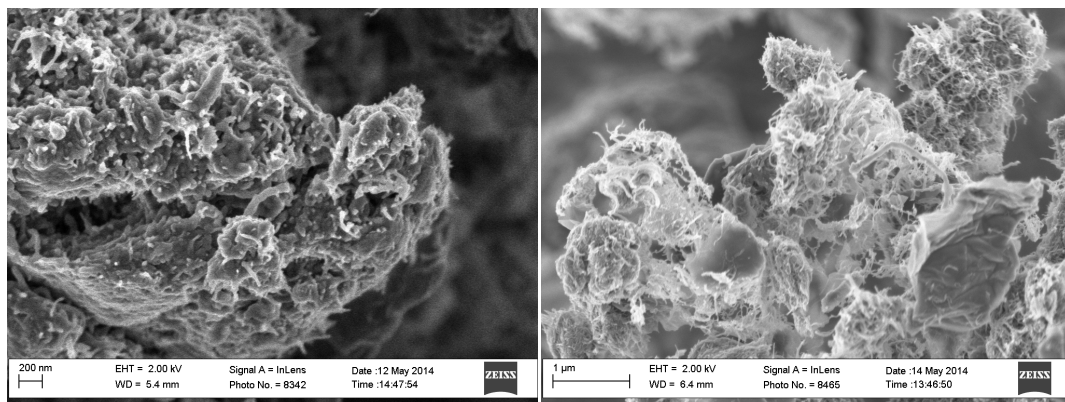
(a)   (b)

Figure 5.7: SEM images of RGO@MWCNT with Dybenzyl Disulfide (heat treated) and mixed Sulfur
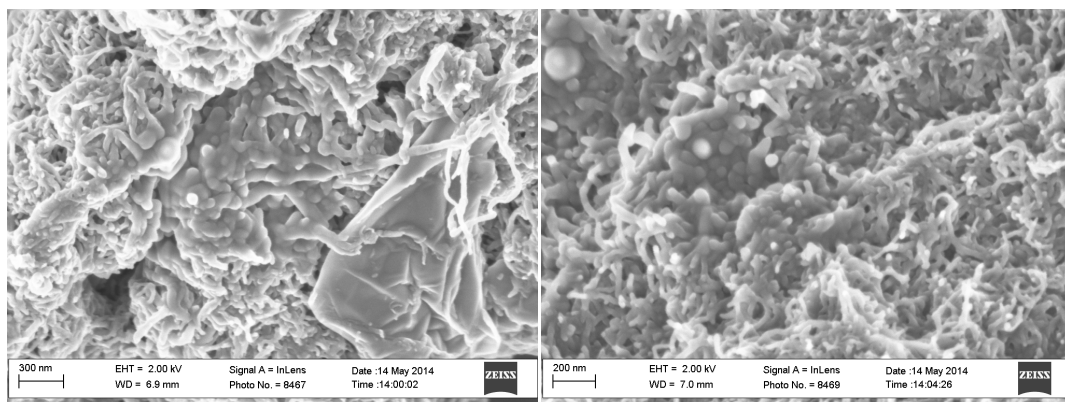
(a)   (b)

Figure 5.8: SEM images of RGO@MWCNT with Dybenzyl (poly) Sulfide

Charging Discharging Characteristics of the Organo Sulfur Based Li-S Cells

The cell characteristics were analyzed and compared with currently available cathode materials for Li-S cells. Initially cell characteristics were measured for Sulfur cathode (against Li anode) which was synthesized using simple mechanical mixing of Sulfur in to

RGO. It was noted that the capacity fading is high due to the poor intercalation of Sulfur in RGO. These poor cell characteristics were similar for Multiwall Carbon Nanotubes when sulfur was mixed mechanically. However the operational theoretical voltage close to 2.53 V was achieved. This voltage of 2.53 V is characteristic for Li$_2$S. A step like discharging curve was observed showing that Li$^+$ forms intermediate polysulfide.
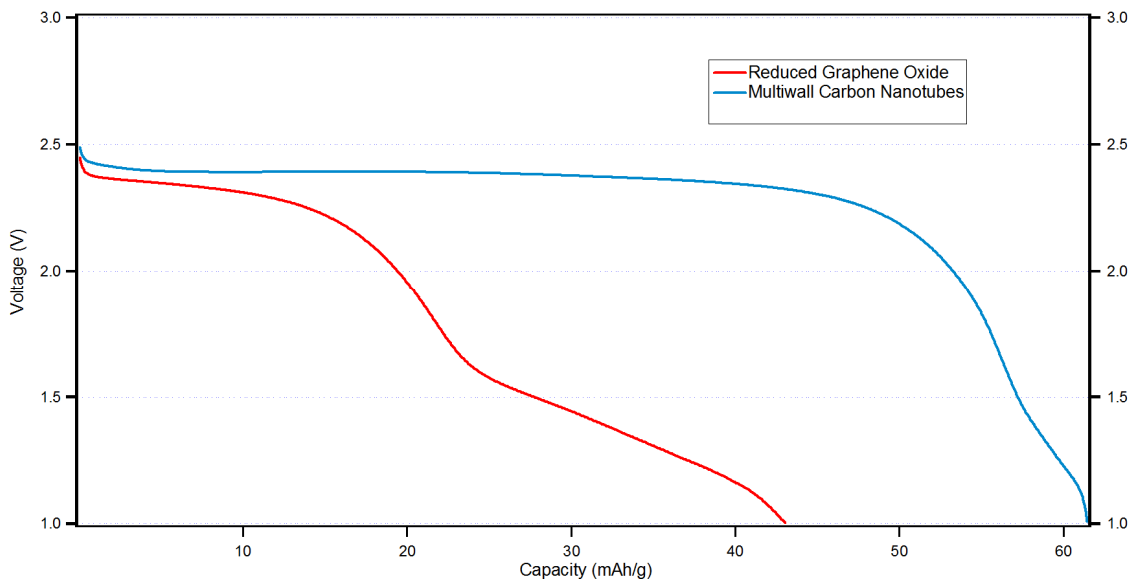

Figure 5.9: First cycle voltage variation with discharge capacity of mechanically mixed Sulfur with RGO and MWCNT (Method 1)

Cathodes which were synthesized by functionalizing of Sulfur in to RGO and Multiwall Carbon Nanotubes were separately tested. In the functionalizing process, Sulfur atoms effectively intercalate among the RGO sheets or MWCNT's compared to mechanically mixing of Sulfur. It was noted that theoretical cell voltage close to 2.53 V is achieved indicating that the Li$_2$S is formed. The first cycle capacity achieved for functionalized RGO with Sulfur is 420 mAh/g and for functionalized MWCNT with Sulfur is 365 mAh/g (figure 5.11).
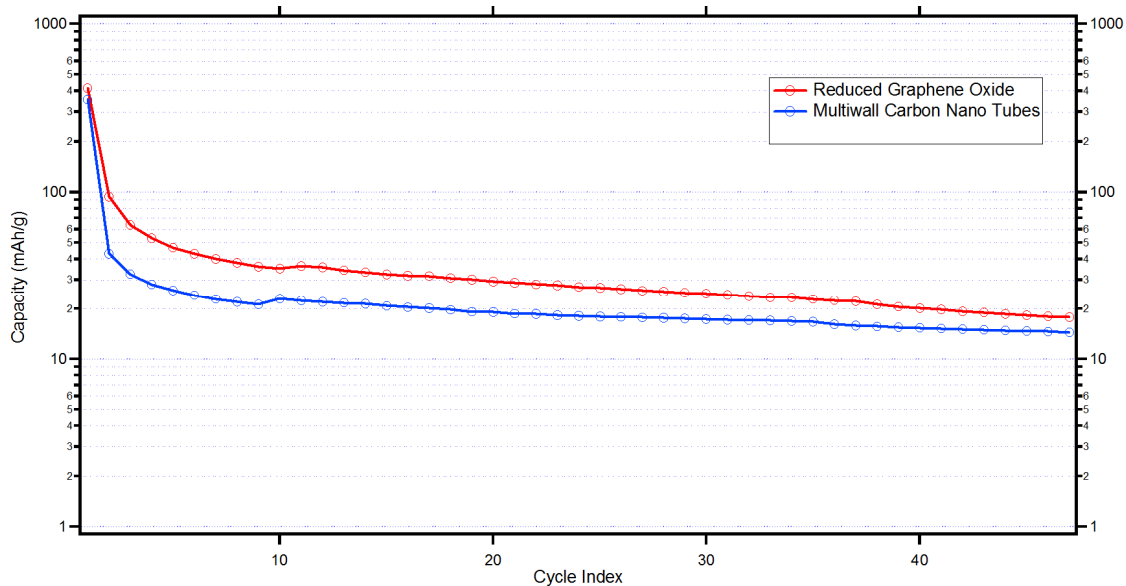
Figure 5.10: Discharge capacity variation with cycle Index of functionalized cathode materials with sulfur (Method 2)
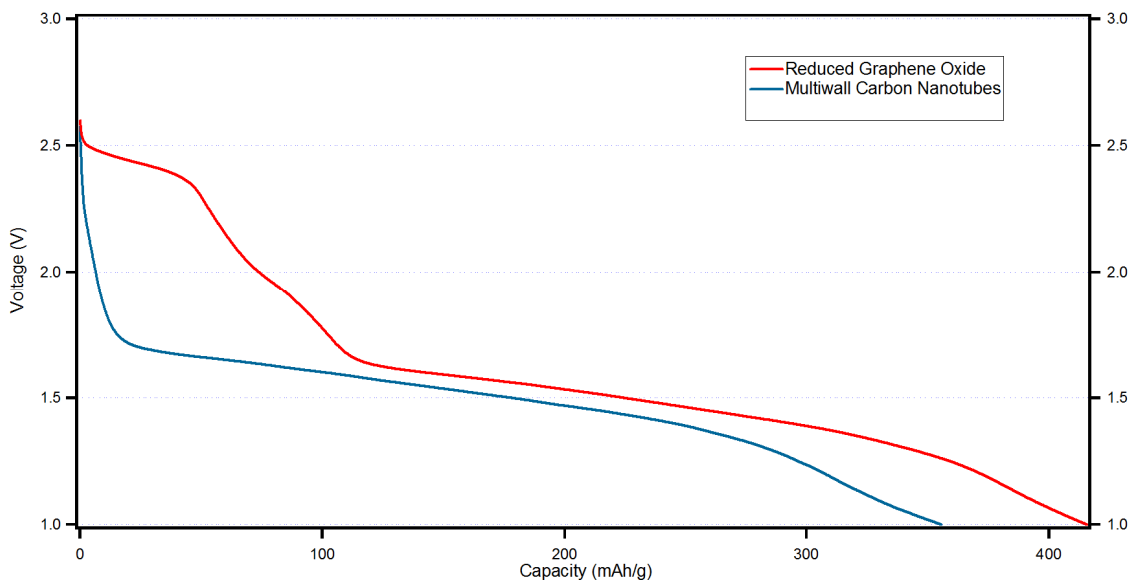

Figure 5.11: First cycle voltage variation with discharge capacity of functionalized cathode materials with sulfur (Method 2)

An improved cell capacity was observed for encapsulated Sulfur by Triton X-100 surfactant. This encapsulating method has been performed as in method 3. The first cycle cell capacity is around 1200 mAh/g (Figure 5.12). However average cell voltage was around 1.6 V indicating that only the Lithium polysulfides are formed (Figure 5.12).
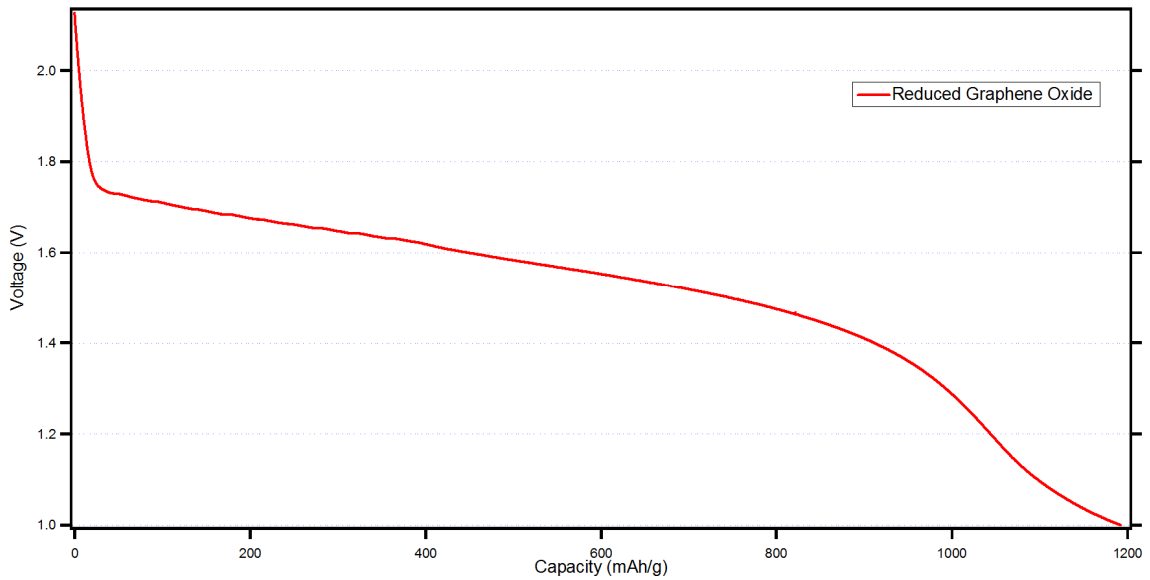

Figure 5.12: First cycle discharge voltage variation with discharge capacity of Sulfur encapsulated cathode material (Method 3)
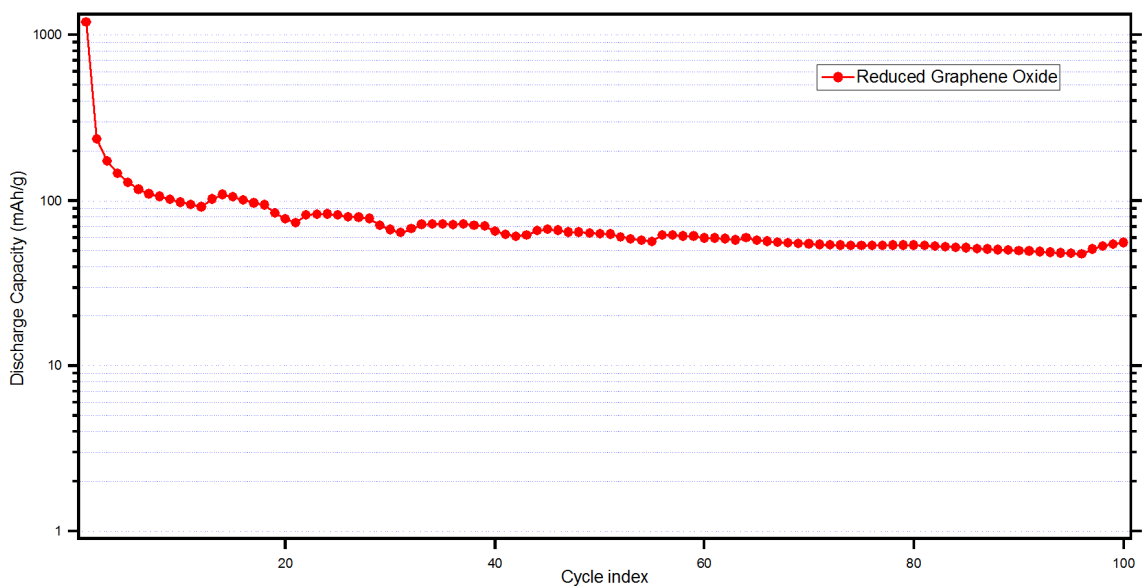
Figure 5.13: Discharge capacity variation with cycle index of Sulfur encapsulated cathode material (Method 3)

Organo Sulfur cathodes were tested with respect to Li anode. Cyclabilty, discharging and charging curves were measured using Arbin 2000 battery tester. Cyclic Voltammetry was also performed. Average voltage obtained was about 1.5 V since most of the Li^+ only react with Ph-CH$_2$-S-. However it was able to maintain 200 mAh/g cell capacity even after 100 cycles showing the effect of Dybenzyle Disulfide as a potential cathode material.
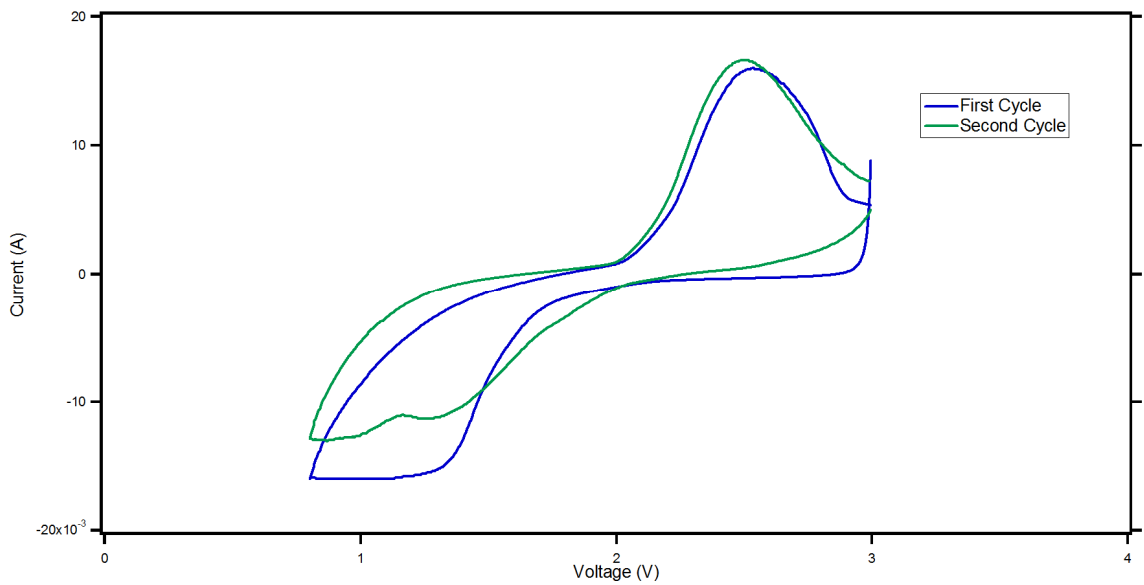
(a)
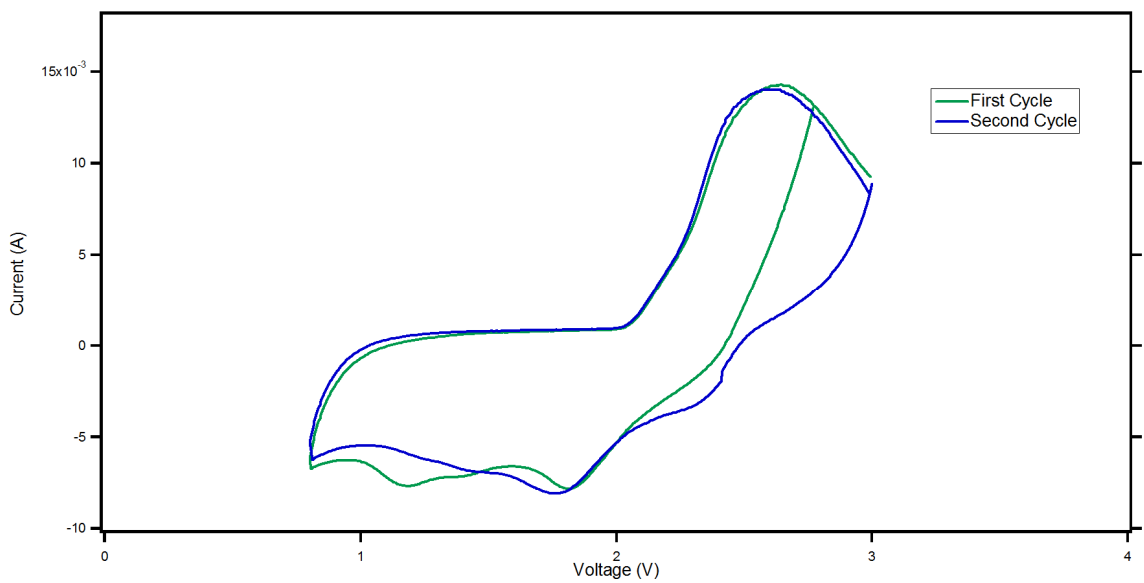
(b)

Figure 5.14: Cyclic voltammetry measurements (a) Dibenzyl Disulfide only RGO@MWCNT cell, (b) Cyclic voltammetry of Dibenzyl Disulfide and Sulfur at RGO@MWCNT cell.

When the two cyclic voltammetry curves are compared, Figure 5.14.b shows better cyclability than figure 5.14.a. Such recyclability is a result of better stability of Benzyl Sulfide group while the cell is being discharged. Further, it proves that the Benzyl group can recombine with sulfur when the cell is being charged by forming polysulfide chain in between Dybenzyl groups. However the Figure 5.14.b shows the peaks at around 1.5 V confirming that polysulfides are also formed. This suggests that cells made via method 4 should be further modified assuring that only tri-sulfur chain exists in between Dibenzyl groups.
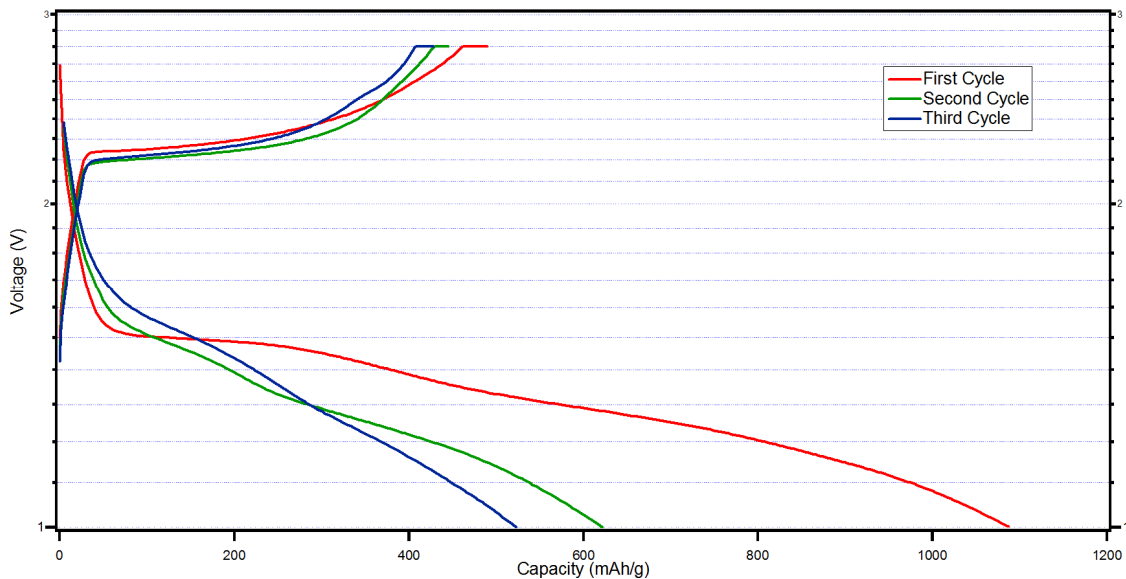

Figure 5.15: Voltage variation with respect to capacity of first three cycles of Dibenzyl Disulfide and Sulfur at RGO@MWCNT cell
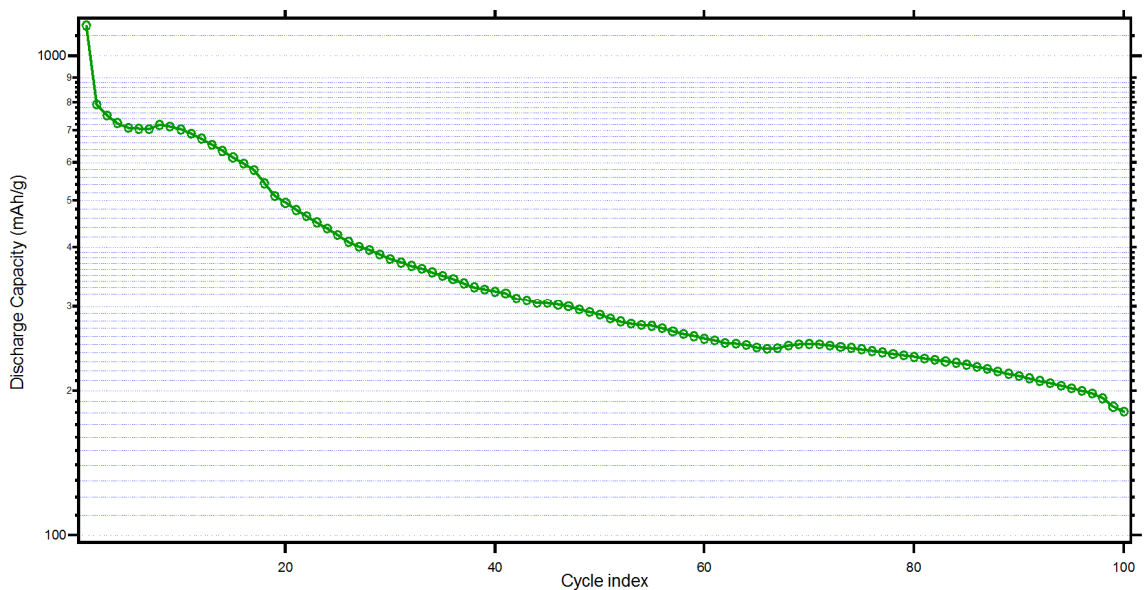
Figure 5.16: Discharge capacity over Cycle number of Dibenzyl Disulfide based cell

In contrast to Dibenzyl Disulfide and Sulfur based cells, DybenzylTrisulfide cells do show higher capacity retain in first twenty cycles showing that DybenzylTrisulfide tends to be oxidized during charging, preventing it going for higher number of cycles. However DubenzylTrisulfide based cells give the better cyclability in the first 20 cycles compared to the all other methods discussed above. Voltage variation upon discharge and recharge is shown in figure 5.18. It reveals the good recyclability of DybenzylTrisulfide based batteries. The cyclic voltammetry curves in Figure 5.19 shows a quasi-reversible reaction.
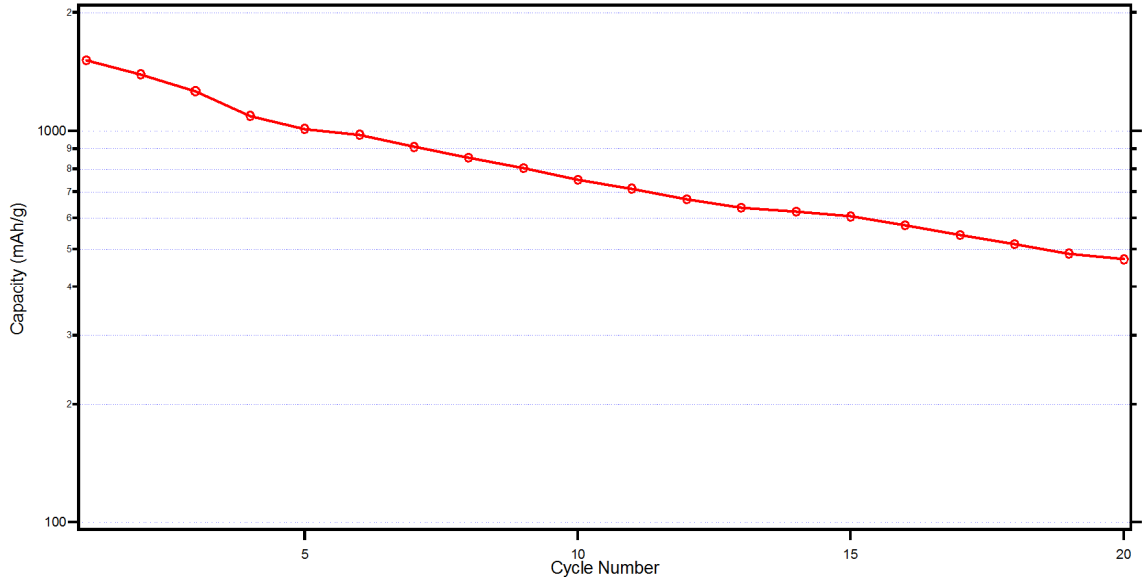
Figure 5.17: Capacity vs Cycle number of DybenzylTrisulfide based Li-S cell
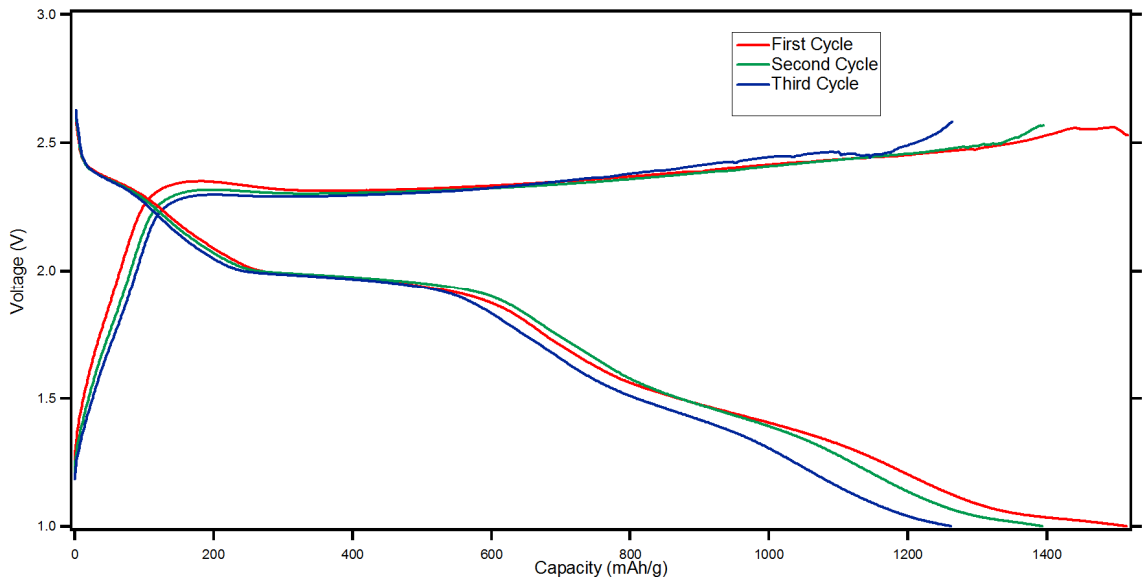

Figure 5.18: Voltage variation upon charging and discharging of DybenzylTrisulfide
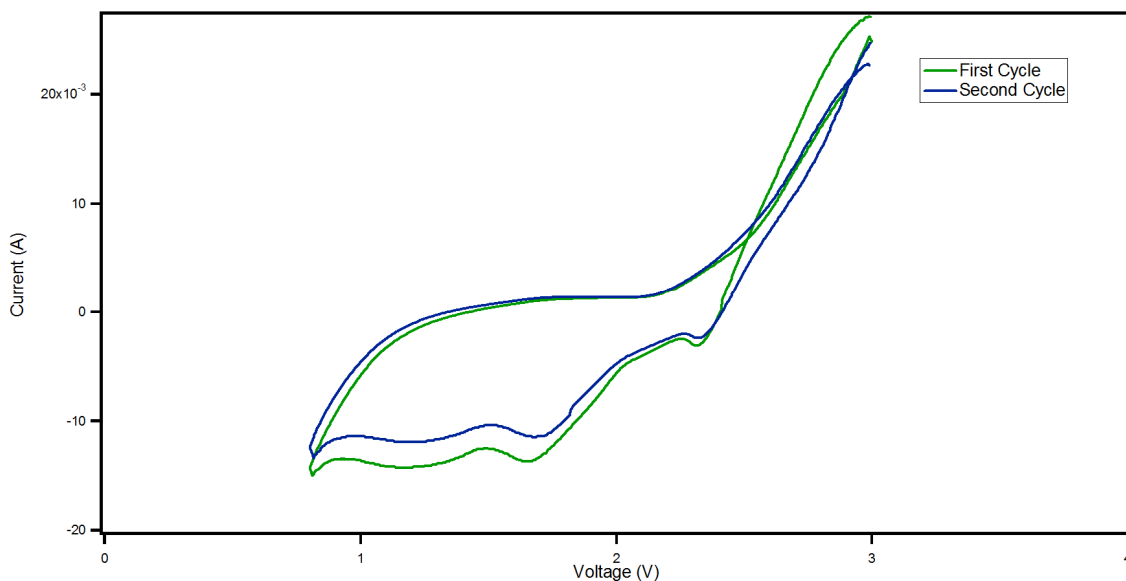
based cell

Figure 5.19: Cyclic voltammetry of DybenzylTrisulfide based cell

Charging Curves of Li-S Cell

Proper charging of Li-S cell is also equally important as discharging performances of Li-S cells. If the cell was overcharged, it may oxidize the active materials affecting its cyclability. Also if the cell is under charged, it also reduces the cyclability due to capacity fading over cycle number. Therefore proper charging is very important for better performances of Li-S cells. In this research overcharging and under charging was prevented by setting appropriate voltage cut off values and current cut off values using Arbin 2000 battery tester. Cut off voltage and current were set to 2.8 V and 500 μA respectively as the charging limits. However, sometimes distorted charging curves were observed in Dibenzyl Disulfide based cells. The reason for such distorted charging curves were found out to be due to the expansion and cracking of the cathode electrode upon charging. Figure 5.20 shows such distorted charging curve. This phenomenon was

45

overcome by physically re-enforcing the cathode materials by sandwiching the RGO@MWCNT structure in between two similar stainless steel meshes.
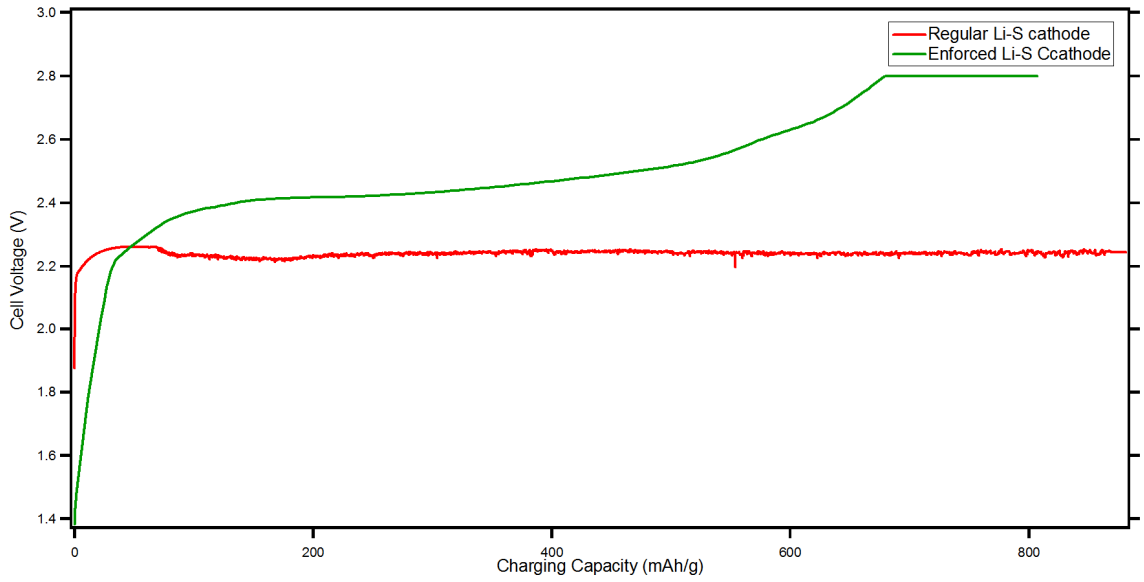

Figure 5.20: Distorted and normal charging curve of DybezylDdisulfide based cell

CONCLUSIONS

Relatively pure, reduced graphene oxide was obtained by reducing graphene oxide with Hydrazine. Therefore Hydrazine can be a good candidate to synthesize reduced graphene oxide in large quantities. Comparison of D and G band intensities can be used to identify the degree of reduction of RGO.

In this work, different methods of intercalating sulfur were attempted. It was concluded that physical confinement allows improvement of the charge conductivity of the sulfur-carbon matrix composite, but at the same time it imposes other difficulties including measurement of correct mass of sulfur in the carbon matrix. Hence the specific capacity reported in the experiments where methods 1, 2 and 3 are employed would have been deviated from their true values.

Use of Oragano Polysulfide in cathode matrix as Sulfur source has shown better results in this work compared to physical Sulfur intercalation. But multiple Sulfur atoms must exist in polysulfur chain between the aromatic rings in order to reach full capacity of the cathode. Minimum number of sulfur atoms that must exist in such a sulfur chain was found to be three. Otherwise the organo polysulfide molecules will undergo 'scissoring' reaction with Lithium without forming Li_2S. This phenomena was proven by cyclic voltammetry measurements (Figure 5.14.a) and using DibenzylTrisulfide as a Sulfur source. In addition it was concluded that, the capacity of Sulfur cathode depends on

number of S—S bonds in methods 4 and 5 described in chapter 3. Cathodes, which were made using DibenzylTrisulfide have shown better results it the first 20 cycles. It can be concluded that existence of three sulfur atoms between two aromatic rings prevents the formation of soluble polysulfide formation in the first stages. However it was unable to stabilize the specific capacity curve at a reasonable value from 20 cycles to 100 cycles. Reasons for this capacity fade are currently not known and require further investigation.

REFERENCES

1. Wang, H., et al., *Graphene-wrapped sulfur particles as a rechargeable lithium-sulfur battery cathode material with high capacity and cycling stability.* Nano Lett, 2011. **11**(7): p. 2644-7.
2. David Linden, T.B.R., *Handbook Of Batteries 3rd Edition.*
3. Dreyer, D.R., et al., *The chemistry of graphene oxide.* Chem Soc Rev, 2010. **39**(1): p. 228-40.
4. Huang, H., et al., *Highly efficient electrolytic exfoliation of graphite into graphene sheets based on Li ions intercalation–expansion–microexplosion mechanism.* Journal of Materials Chemistry, 2012. **22**(21): p. 10452.
5. Wang, G., et al., *Graphene nanosheets for enhanced lithium storage in lithium ion batteries.* Carbon, 2009. **47**(8): p. 2049-2053.
6. Song, M.K., Y. Zhang, and E.J. Cairns, *A long-life, high-rate lithium/sulfur cell: a multifaceted approach to enhancing cell performance.* Nano Lett, 2013. **13**(12): p. 5891-9.
7. Xiao, M., et al., *Sulfur@graphene oxide core–shell particles as a rechargeable lithium–sulfur battery cathode material with high cycling stability and capacity.* RSC Advances, 2013. **3**(15): p. 4914.
8. Maddanimath, T., et al., *Self-assembled monolayers of diphenyl disulphide: a novel cathode material for rechargeable lithium batteries.* Journal of Power Sources, 2003. **124**(1): p. 133-142.
9. Oae, S., *Organic Sulfur Chemistry: Structure and Mechanism.* 1991.
10. Xie, J., et al., *Preparation of three-dimensional hybrid nanostructure-encapsulated sulfur cathode for high-rate lithium sulfur batteries.* Journal of Power Sources, 2014. **253**: p. 55-63.
11. Ash, D.K., *The chemistry of organic trisulfides and related derivatives.* 1973.
12. Smith, R.A., *The desulfurization of organic trisulfides a mechanistic study.* 1979.
13. E.T.Aayodele, A.A.O., *Synthesis of subsitituted benzyl phthalamido disulphmides.* Chemical Society of Ethiopia, 1999. **13**: p. 1011-3294.

CURRICULUM VITAE

NAME: Ruchira Ravinath Dharmasena

ADDRESS: Department of Physics & Astronomy
                      102 Natural Science Building
                      University of Louisville
                      Louisville, KY 40292

DOB: September 26, 1984

EDUCATION: BSc, Physics
                      University of Peradeniya, Sri Lanka.
                      2005-2009

                      MS, Physics
                      University of Louisville
                      Louisville, KY 40292.
                      2012-2014

PUBLICATIONS:

1. Li Zhu, **R. Dharmasena**, S. McNamara, *MOS tunneling strain sensor using an AC measurement technique,* Nano/Micro Engineered and Molecular Systems (NEMS), 2013 8th IEEE International Conference

2. Ruwantha Jayasinghe, Arjun Kumar Thapa**, Ruchira R. Dharmasena**, Tu Quang Nguyen, Bhabendra K. Pradhan, Hem Sharma Paudel, Jacek B. Jasinski, Andriy Sherehiy, Masaki Yoshio, G.U. Sumanasekera, *Optimization of Multi-Walled Carbon Nanotube based CFx electrodes for improved primary and secondary battery performances*, Journal of Power Sources 2014, 253, 404–411

3. I. M. Dharmadasa, P. A. Bingham, O. K. Echendu, H. I. Salim, T. Druffel, R. Dharmadasa, G. U. Sumanasekera, **R. R. Dharmasena**, M. B. Dergacheva, K. A. Mit, K. A. Urazov, L. Bowen, M. Walls and A. Abbas, *Fabrication of*